Nuclear magnetic resonance analysis and activation energy spectrum of the irreversible structural relaxation of amorphous zirconium tungstate

F. Miotto,[1] G. L. Rech,[1,2] A. M. Turatti,[2,3] J. Catafesta,[1] J. E. Zorzi,[1] A. S. Pereira,[4] and C. A. Perottoni[1,*]

[1]*Universidade de Caxias do Sul, 95070-560 Caxias do Sul, Rio Grande do Sul, Brazil*

[2]*PGCIMAT, Universidade Federal do Rio Grande do Sul, 95070-560 Porto Alegre, Rio Grande do Sul, Brazil*

[3]*Universidade Federal de Rio Grande, 96203-900 Rio Grande, Rio Grande do Sul, Brazil*

[4]*Universidade Federal do Rio Grande do Sul, 95070-560 Porto Alegre, Rio Grande do Sul, Brazil*

(Received 16 December 2017; published 13 March 2018)

Zirconium tungstate undergoes a sequence of phase transitions from cubic (α-ZrW_2O_8) to orthorhombic (γ-ZrW_2O_8) to amorphous (a-ZrW_2O_8) upon increasing pressure at room temperature. The amorphous phase is known to undergo anomalous endothermic recrystallization into a high-temperature β-ZrW_2O_8 phase above 600 °C at ambient pressure (and back to α-ZrW_2O_8 when brought to room temperature). The endothermic recrystallization of a-ZrW_2O_8 is preceded by an irreversible exothermic structural relaxation. New W-O bonds are formed upon amorphization, continuing a tendency of increasing W coordination number in going from α to γ-ZrW_2O_8. In fact, contrarily to α-ZrW_2O_8, in which one-quarter of the oxygen atoms are bonded only to one W (terminal oxygens), previous works found no evidence of single-bonded oxygen atoms in a-ZrW_2O_8. It thus could be argued that the irreversible character of the structural relaxation of a-ZrW_2O_8 is due to W-O bond breaking upon annealing of the amorphous phase. To test this hypothesis, x-ray diffraction, ^{17}O magic-angle spinning NMR, Raman, and far-infrared analyses were performed on samples of amorphous zirconium tungstate previously annealed to increasingly higher temperatures, looking for any evidence of features that could be assigned to the presence of terminal oxygen atoms. No evidence of single-bonded oxygen was found before the onset of recrystallization. Furthermore, the kinetics of the structural relaxation of a-ZrW_2O_8 is consistent with a continuous spectrum of activation energy, spanning all the range from 1 to 2.5 eV. These findings suggest that the structural relaxation of amorphous zirconium tungstate, however irreversible, is not accompanied by W-O bond breaking, but most probably characterized by a succession of (mostly) irreversible local atomic rearrangements.

DOI: 10.1103/PhysRevB.97.094203

I. INTRODUCTION

Zirconium tungstate (α-ZrW_2O_8) is a widely known ceramic material that contracts isotropically when heated [1,2]. Besides isotropic negative thermal expansion (NTE), zirconium tungstate also exhibits anomalous high heat capacity and low thermal conductivity at low temperature, as well as stiffening (i.e., bulk modulus increase) with increasing temperature [3–6]. Above 156 °C, at ambient pressure, α-ZrW_2O_8 undergoes an order-disorder transition to β-ZrW_2O_8 with just a minor change in the linear thermal expansion coefficient [2]. At pressures above 0.2 GPa and room temperature, zirconium tungstate transforms irreversibly into an orthorhombic phase which also exhibits NTE [7–9]. By further increasing pressure above 1.5 GPa, zirconium tungstate undergoes pressure-induced amorphization (PIA) and, upon heating at ambient pressure, amorphous zirconium tungstate (a-ZrW_2O_8) undergoes an irreversible exothermic structural relaxation followed by an unusual endothermic recrystallization [10–13].

The crystal structure of α-ZrW_2O_8 at room temperature and pressure can be described as a three-dimensional corner-sharing array of ZrO_6 octahedra and WO_4 tetrahedra. In each WO_4 tetrahedron, one of the four oxygen atoms (the terminal oxygen) is not bonded to the neighbor zirconium. The nonbridging, terminal oxygen allows the α-ZrW_2O_8 crystal structure to respond to stress with minimum potential energy variation (zero, in the strict limit of rigid bonds). Accordingly, α-ZrW_2O_8 is referred to as a topologically soft framework structure.

Negative thermal expansion in ZrW_2O_8 has been attributed to low-energy, transverse vibrational modes [also called rigid unit modes (RUMs)], involving tilting of nearly rigid polyhedra, whose increase in amplitude leads to contraction upon heating [14–16]. However, details of the mechanism responsible for NTE in this compound are still controversial [17–22]. The same can be said about the mechanism responsible for PIA [10,12,23–26]. In previous works we have assumed that both phenomena (NTE and PIA) have a common origin in some low-energy rigid unit modes [10,20]. Indeed, the hypothesis is that, in the case of zirconium tungstate, a large number of low-energy modes would simultaneously soften at high pressures, thus destabilizing the structure and leading to the formation of a high-pressure disordered phase [24,27]. New W-O bonds are formed upon amorphization, thus contributing to the metastable retention of the amorphous phase at room pressure [10,28].

The increase of tungsten coordination number with the formation of new W-O bonds in a-ZrW_2O_8 decreases the number of motional degrees of freedom, hindering

*caperott@ucs.br

transverse low-energy vibrational modes to such an extent that amorphous zirconium tungstate becomes a positive thermal expansion material [12]. Indeed, x-ray photoelectron spectroscopy (XPS) results indicate that there are no terminal oxygens in a-ZrW_2O_8, thus giving support to the hypothesis of W-O bond formation upon pressure-induced amorphization of zirconium tungstate [28]. Dilatometric analysis of amorphous zirconium tungstate showed that this material undergoes an irreversible structural relaxation when heated above room temperature [12,25]. Moreover, temperature-modulated differential scanning calorimetry (TMDSC) experiments have shown an anomalous endothermic recrystallization of the amorphous phase, which is preceded by an exothermic relaxation [11,13]. A preliminary Daniel-Borchardt analysis of the heat evolved during the irreversible structural relaxation of amorphous zirconium tungstate suggested that the kinetics of this process cannot be adequately described by a single activation energy but may involve a continuous activation energy spectrum [13]. Indeed, as with other amorphous solids, the kinetics of the structural relaxation of a-ZrW_2O_8 may not be characterized by a single activation energy [29,30].

Despite relaxation and recrystallization of a-ZrW_2O_8 having been subject to study before (see, for instance, Refs. [10,11,13,31–33]), some issues remain unclear. We do not know, for instance, to what extent bond breaking (particularly W-O bond breaking) is involved and may ultimately be responsible for the irreversible nature of the a-ZrW_2O_8 structural relaxation. Accordingly, in this work, local structure analysis techniques, namely magic-angle spinning nuclear magnetic resonance of ^{17}O (MAS NMR), Raman, and far-infrared spectroscopy, were used to probe samples of amorphous zirconium tungstate previously annealed to increasingly higher temperatures, looking for evidence of the presence of terminal oxygens. Indeed, the cumulative breaking of the W-O bonds formed upon pressure-induced amorphization of zirconium tungstate could explain the irreversible character of the structural relaxation of this amorphous compound. Furthermore, the spectrum of activation energy for the relaxation of a-ZrW_2O_8 was determined by solving the Primak model inverse problem, applying Tikhonov's regularization to temperature-modulated differential scanning calorimetry data [34–36]. This approach allowed us to infer the nature and the activation energy range of the local atomic rearrangements responsible for the irreversible structural relaxation before the endothermic recrystallization of amorphous zirconium tungstate.

II. EXPERIMENTAL

The a-ZrW_2O_8 samples used in this work were prepared by pressing pellets of α-ZrW_2O_8 (Wah Chang Co., Albany, OR) to 7.7 GPa at room temperature, for 2 hours, in a toroidal high-pressure chamber [10,37–39]. Pre-compacted samples were enclosed into hexagonal boron nitride (hBN) capsules to ensure *quasi*-hydrostatic conditions. These hBN capsules were capped with hBN and pyrophyllite disks and inserted into a graphite cylinder. This whole set was then put into a ceramic gasket that works as sealing between the two parts of the toroidal-type chamber. Pressure calibration was performed using Bi transition pressures as fixed points [38]. The sharp Bi transitions observed during calibration runs suggest this experimental assembly provides reasonably isostatic conditions up to (at least) 7.7 GPa at room temperature. A cylindrical sample of solid amorphous zirconium tungstate, with approximately 6 mm diameter, is obtained after pressure release. Amorphous zirconium tungstate was then carefully ground in an agate mortar to provide powder samples suitable for x-ray diffraction, modulated differential scanning calorimetry analysis, and vibrational and nuclear magnetic resonance spectroscopy.

A. X-ray diffraction

Powder x-ray diffraction analysis was used to assess the crystalline/amorphous state of samples and also to follow the structural evolution of samples previously heated up to some predefined temperature. Measurements were performed at room temperature in a Shimadzu XRD 6000 diffractometer in Bragg-Brentano geometry, with Cu Kα radiation ($\lambda = 1.5405$ Å), a 1 ° divergence slit, a 1° scattering slit, a 0.30 mm reception slit, and a graphite monochromator in the scattered beam. The step size and acquisition time were 0.05° and 4 seconds per step, respectively. Measurements were made using a powder sample on top of a nearly background-free silicon single crystal oriented in the [511] direction. Rietveld analysis of the α-ZrW_2O_8 x-ray powder pattern was performed using FULLPROF [40].

B. MAS NMR spectroscopy

Solid-state, magic-angle spinning nuclear magnetic resonance spectroscopy of ^{17}O nuclei in zirconium tungstate used approximately 1 g of α-ZrW_2O_8 that was first isotopically enriched with ^{17}O as described elsewhere [41]. X-ray powder diffraction was used to check the crystal structure of the sample after ^{17}O enrichment. The α-ZrW_2O_8 ^{17}O-enriched sample was submitted to NMR analysis using a 500 MHz Agilent spectrometer with a magnetic field of 11.7 T at 67.8 Hz. The chemical shift was measured taking the signal of $H_2{}^{17}O$ (natural abundance) as a reference. The sample was packed into a 4.0 mm diameter zirconia rotor and measurements were carried out with sample rotating at 10 kHz. Room-temperature NMR spectra of ^{17}O-enriched amorphous zirconium tungstate samples (as obtained and after successive annealings at increasingly higher temperatures) were obtained with a Bruker 600 MHz spectrometer operating with a magnetic field of 14.1 T at 81.4 Hz. As before, NMR chemical shift was calibrated against $H_2{}^{17}O$ (natural abundance). For this analysis, amorphous ZrW_2O_8 samples were packed into a 2.5 mm diameter zirconia rotor, which was rotating at 25 kHz during analysis. The annealings of a-$ZrW_2{}^{17}O_8$ before room-temperature ^{17}O MAS NMR measurements were carried out under an ultrapure nitrogen atmosphere, using a 2 $Kmin^{-1}$ heating rate and 5 min holding time at maximum temperature.

C. Vibrational spectroscopy

Vibrational spectroscopy techniques (Raman scattering and Fourier-transformed infrared absorption spectroscopy) were used to investigate the presence of low-energy vibrational modes of zirconium tungstate. Raman spectra were obtained at room temperature using a backscattering geometry in an

Olympus BXFM microscope (with a 50× objective) attached to a Horiba LabRam Evolution HR800 spectrometer, using a HeNe laser (632.81 nm), a 600 lines per millimeter grating, and a Peltier-cooled CCD detector operating at −70 °C. Fourier-transformed far-infrared absorption spectra from 150 to 20 cm^{-1} were obtained with a Vertex 70V Bruker FTIR spectrometer, with samples diluted in high-density polyethylene (HDPE) powder. The FTIR spectra were obtained with the spectrometer optics and sample compartment both under a vacuum, at room temperature. Each spectra comprised 2000 scans at 4 cm^{-1} resolution.

D. Temperature-modulated differential scanning calorimetry

Temperature-modulated differential scanning calorimetry (TMDSC) analysis was carried out with a Netzsch 204 F1 Phoenix heat flux scanning calorimeter. Measurements were performed with about 40 mg of a-ZrW_2O_8 enclosed in a platinum crucible with lid, with an empty Pt crucible as a reference. The DSC furnace was purged with 20 mL min^{-1} of high-purity argon (5 N, from Air Products). The heating rate was set to 3 Kmin^{-1} and the amplitude and period of the sinusoidally modulated temperature were set to 1 K and 120 s, respectively.

The nonreversible heat flow component of the total DSC signal was used to obtain the activation energy spectrum for the structural relaxation of a-ZrW_2O_8. Measurements were carried out in triplicate, from 353 K to 873 K. The averaged nonreversible signal from the second and third scans was taken as the baseline and subtracted from the first signal to yield the heat flow due to the irreversible relaxation of amorphous zirconium tungstate. The relaxation progress (α) was obtained as the ratio of the irreversible heat Q_i released by the sample up to a given temperature T_i to the total irreversible heat released in the process, Q_∞, $\alpha_i = Q_i/Q_\infty$. The heat released by the sample is obtained as the integral of the nonreversible MDSC signal. The relaxation progress was thus obtained as a function of temperature by fitting an empirical expression,

$$\alpha(T) = N - \sum_{i=1}^{N} 2^{-p_i}\left(\mathbf{1} + \mathrm{erf}\left\{-\sigma_i^2 \ln\left[B_i(x-\mu_i)\right]\right\}\right)^{p_i}. \tag{1}$$

The above expression, with $N = 2$, was fitted to the set of α_i data using a differential evolution algorithm [42]. Fitting parameters included all p_i, B_i, μ_i, and σ_i. The resulting expression was then used in the solution of the inverse problem, as described below.

E. Kinetics of energy-distributed processes

For a structural relaxation, in which the rate of kinetic processes dq/dt is dependent on the number of available processes q to the power of the reaction order n [34],

$$-\frac{dq}{dt} = k\,q^n. \tag{2}$$

Here k, the frequency factor, is a function of temperature (typically an Arrhenius expression of the activation energy). The number of available processes, however, cannot be directly measured and, accordingly, another property (or property change) of the system, p, which is dependent on q through $p = fq$, is actually measured. Equation (2) then becomes

$$-\frac{dp}{f\,dt} = k_0\, e^{-\frac{\epsilon}{k_B T}}\left(\frac{p}{f}\right)^n, \tag{3}$$

where ϵ is the activation energy, T is the absolute temperature, k_B is the Boltzmann constant, and k_0 is a constant with units of frequency. In what follows we will assume that the structural relaxation of amorphous zirconium tungstate can be well described by a first-order ($n = 1$) kinetics of successive local, single-step atomic rearrangements. Given that the structural relaxation of a-ZrW_2O_8 occurs over a wide temperature range, actual experimental determinations of the reaction progress are carried out by varying temperature, which then becomes a function of time. In experiments conducted at a constant heating rate, temperature and time are related by $t = \beta T$, where β is a constant with units of seconds per kelvin. Under these assumptions, Eq. (3) can be written as [34]

$$p = p_0\, e^{-k_0 \beta T E_2\left(\frac{\epsilon}{k_B T}\right)}, \tag{4}$$

where $E_2(x) = x\int_x^\infty e^{-t}t^{-2}dt$. In the present case, the processes are distributed in activation energy so both p (the response of the system due to processes for which the energy barriers have been overcome at a given temperature) and p_0 (the probability density of possible processes as a function of its activation energies) are distribution functions. The property P that is actually measured depends on all isolated events that contribute to the structural relaxation and is, therefore, given by the overall response to all available processes for a given temperature T, i.e.,

$$P = \int_0^\infty p(\epsilon)d\epsilon = \int_0^\infty p_0\, e^{-k_0 \beta T \mathbf{E}_2\left(\frac{\epsilon}{k_B T}\right)}d\epsilon. \tag{5}$$

Expressed in terms of the progress of the structural relaxation, $\alpha(T)$, Eq. (5) becomes

$$1 - \alpha(T) = \int_0^\infty p_0(\epsilon)\, e^{-k_0 \beta T \mathbf{E}_2\left(\frac{\epsilon}{k_B T}\right)}d\epsilon. \tag{6}$$

The function of interest, p_0, is a probability density function and, as such, must comply with the normalization condition, $\int_{-\infty}^{\infty} p_0(\epsilon)d\epsilon = 1$. Equation (6) is a Fredholm's integral equation of the first kind, which has the general form $g(s) = \int f(t)K(s,t)dt$, where $K(s,t)$ is the *kernel* (a known function that describes the system's behavior), and $g(s)$ is the measured system's response that depends on some intrinsic property of the system described by $f(t)$, the unknown function.

F. Inverse problems

The integral equation (6) can be converted into a linear algebra problem by Galerkin's discretization [43]. However, given that the kernel has the property to smooth the response obtained from the unknown function, the solution space has nontopological characteristics; i.e., it is an ill-posed problem where small variations (such as measurement errors) on the response function can result in entirely different activation energy spectra. To help solve this issue, Tikhonov's regularization was used to work around the intrinsic instability of the inverse problem.

Tikhonov's regularization (also called Tikhonov-Phillips' regularization) is the most widely used direct method for the solution of discrete ill-posed problems [35,36]. After Galerkin discretization, the problem of solving the integral equation (6) is converted into solving a matrix equation, $A\mathbf{x} = \mathbf{b}$. Problems of this type are usually trivial, even if, due to unavoidable measurement errors, an exact solution is out of reach. The solution, instead, becomes the vector $\mathbf{x}_\lambda$ that minimizes the norm of the difference between the data and the model. If A is an exact matrix and the only element containing noise is the vector $\mathbf{b}$, the solution is given by solving the least-squares problem [44]

$$\mathbf{x}_\lambda = \min_{\mathbf{x}} \{\|A\mathbf{x} - \mathbf{b}\|_2\}, \tag{7}$$

where A is an m by n matrix, $\mathbf{b}$ is a vector with m elements, and $\|\cdot\|$ represents the vector norm in the Euclidean space. In this study, however, the matrix A has a very large condition number, meaning that the elements of $\mathbf{x}$ will be unavoidably contaminated with noise and will exhibit a large variance, no matter how subtle the perturbations on the measured data (i.e., on the elements of $\mathbf{b}$) [35,36]. In Tikhonov's regularization, a parameter λ is used to restrict the norm of the solution vector. The least-squares problem then takes the form

$$\mathbf{x}_\lambda = \min_{\mathbf{x}} \{\|A\mathbf{x} - \mathbf{b}\|_2 + \lambda\|L\mathbf{x}\|_2\}, \tag{8}$$

where L is a discrete differential operator, used to impose some restriction on the variation amplitude of the solution, although it is often taken as the identity matrix [45]. The regularization parameter λ limits the sensitivity of $\mathbf{x}_\lambda$ to noise. A too small λ makes the solution noisy, while a large value smoothes the solution at the cost of a large residue. The regularization parameter can be chosen as the value corresponding to the corner of a log-log plot of the solution norm $\|\mathbf{x}_\lambda\|_2$ against the residual norm $\|A\mathbf{x} - \mathbf{b}\|_2$ parametrized by λ, also known as the L curve [46]. An appropriate choice for λ thus maintains the balance between the norms, allowing one to reduce the norm of the solution while not permitting the norm of the residue to increase too much.

The spectrum of activation energy for the relaxation of zirconium tungstate was obtained by solving Eq. (6) for $p_0(\epsilon)$. The response function, $g(T) = 1 - \alpha(T)$, was obtained from Eq. (1) as fitted to $\alpha(T)$ data. Using Galerkin's discretization, the kernel function was discretized to a 64×64 square matrix and the empirical expression describing the system's response was discretized to a 64-element vector. Tikhonov's regularization was applied as implemented in the computational package REGULARIZATION TOOLS [47]. The compact form of the singular value decomposition of A was first computed using csvd(). The regularization parameter was then found through the L-curve method using the l_curve() routine. Finally, the regularized solution vector was obtained using the tikhonov() routine, which applies the Tikhonov method for the regularization of the solution based on the matrix A, the system's response $\mathbf{b}$, the previously determined regularization parameter λ, and taking L as the identity matrix.

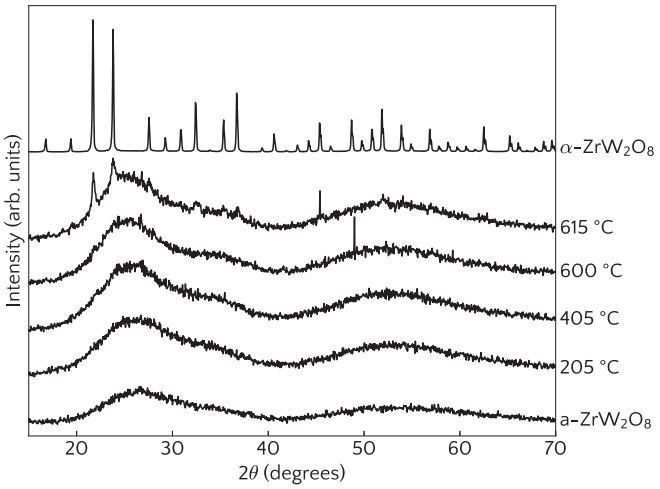

FIG. 1. Room-temperature, x-ray diffraction patterns of (top) pristine α-ZrW_2O_8 and, starting from the bottom, amorphous zirconium tungstate as prepared at high pressure (a-ZrW_2O_8) and after successive heat treatments at increasingly higher temperatures.

III. RESULTS AND DISCUSSION

A. X-ray powder diffraction

Room-temperature, x-ray diffraction patterns of pristine α-ZrW_2O_8 and amorphous zirconium tungstate (as prepared at high pressure and after successive heat treatments at increasingly higher temperatures) are shown in Fig. 1. Rietveld analysis of the x-ray diffraction pattern of the starting powder of α-ZrW_2O_8 yields a lattice parameter $a = 9.1524(1)$ Å, which is in good agreement with the literature [2].

The x-ray diffraction patterns of samples of amorphous zirconium tungstate previously heated up to 600 °C show no distinct Bragg peaks. In fact, the two most intense Bragg peaks from α-ZrW_2O_8 become apparent only in the room-temperature x-ray diffraction pattern of the sample of a-ZrW_2O_8 previously heated to 615 °C. This observation corroborates once more that the nonreversible exothermic DSC signal previously observed in TMDSC experiments carried out up to 600 °C cannot be possibly related to recrystallization of a-ZrW_2O_8 into α-ZrW_2O_8, but only to local rearrangements of the amorphous structure, without long-range ordering [13].

B. MAS NMR spectroscopy

Solid-state magic-angle spinning ^{17}O nuclear magnetic resonance analysis was performed to investigate the occurrence of metal-oxygen bond breaking (more specifically, W-O bond breaking) during relaxation of amorphous zirconium tungstate. Figure 2 presents the room-temperature ^{17}O MAS NMR spectra of isotopically enriched α-ZrW_2O_8 and, also, amorphous zirconium tungstate as obtained and after successive heat treatments at increasingly higher temperatures. The contribution from the four distinct oxygen atoms can be identified in the α-ZrW_2O_8 NMR spectrum at the top of Fig. 2. These oxygen atoms occupy distinct crystallographic sites in the α-ZrW_2O_8 unit cell (space group $P2_13$) and are labeled as O1 (Wyckoff position 12b), O2 (12b), O3 (4a), and O4 (4a), these two latter being terminal oxygens.

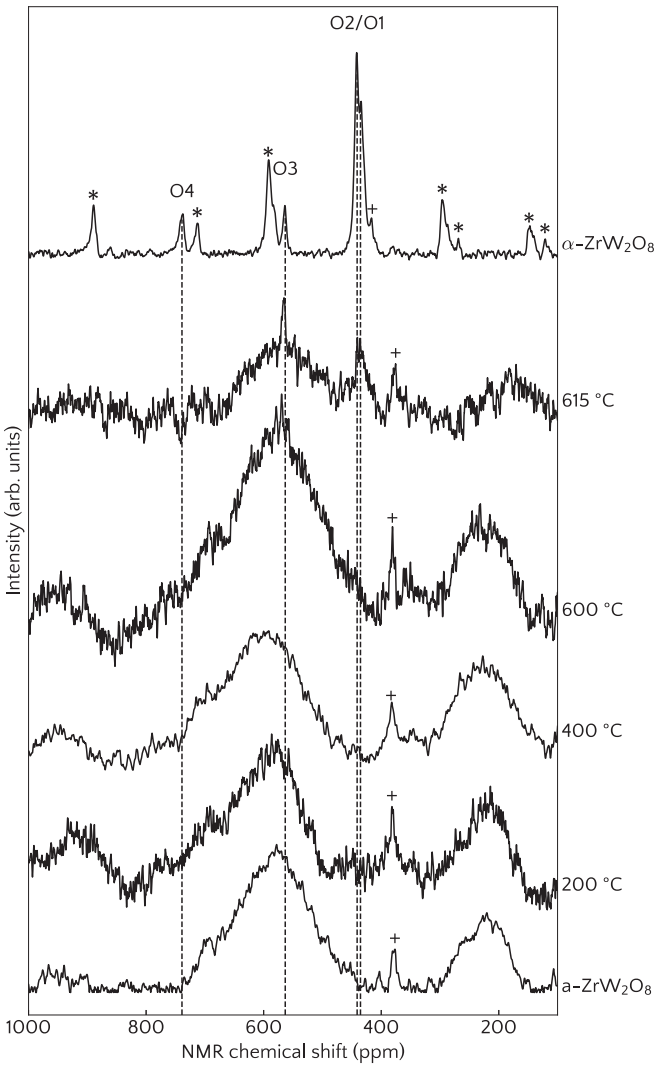

FIG. 2. Room-temperature MAS NMR ^{17}O spectra of α-ZrW_2O_8 and amorphous ZrW_2O_8 as produced and after successive treatments at increasingly higher temperatures, as indicated at right. Asterisks mark lateral bands, and the plus signs indicate rotor bands. Vertical dashed lines mark the NMR chemical shift corresponding to the oxygen bands in the NMR spectrum of α-$ZrW_2{}^{17}O_8$.

The terminal oxygen O4, with coordination number equal to 1, is the less shielded oxygen in the α-ZrW_2O_8 structure, thus giving rise to the ^{17}O NMR band with higher chemical shift, at 739 pm. The O3 is located in a W1-O3-W2 asymmetric environment (W1-O3 and W2-O3 distances are equal to 2.386(9) Å and 1.733(8) Å, respectively [2]) and, therefore, is expected that its resonance signal, at 564 pm, to be found in between the O4 and the O1/O2 NMR bands. Both O1 and O2 atoms are in similar chemical environments (Zr-O-W) and thus give rise to partially overlapping peaks near 438 pm. Besides that, a large number of sidebands can be observed (marked with asterisks) as a consequence of satellite transitions, resembling results previously reported by Hampson *et al.* [41].

The NMR spectrum of amorphous zirconium tungstate shows only a single broad resonance centered at 580 pm, thus indicating that all oxygen atoms are in similar chemical environments and, accordingly, it is no longer possible to distinguish O1, O2, O3, and O4 [48]. There are no significant changes in the room-temperature NMR spectra of a-$ZrW_2{}^{17}O_8$ after annealing at progressively increasing maximum temperatures up to 400 °C, except for a small displacement of the broad band toward slightly higher chemical shift. Comparing the NMR spectra of samples previously heated to 400 °C and 600 °C, i.e., near the recrystallization threshold, it is possible to observe in the latter a shift towards the position of the O3 band in the α-$ZrW_2{}^{17}O_8$. Besides that, it is also possible to notice a subtle hint of the presence of the NMR bands assigned to O3 and O1/O2 atoms. Furthermore, the ^{17}O NMR band measured for the sample of a-$ZrW_2{}^{17}O_8$ previously heated to 600 °C is about 10% broader than the corresponding NMR band measured for amorphous zirconium tungstate as obtained from high-pressure processing. This broader NMR band indicates that the oxygens are subjected to a more varied chemical environment in the sample previously heated to a temperature near the recrystallization threshold as compared to the sample of zirconium tungstate as amorphized.

In the NMR spectrum of a sample of a-$ZrW_2{}^{17}O_8$ previously annealed at 615 °C, in which the recrystallization process has already begun, bands assigned to O1/O2 and O3 are clearly visible. The absence of a signal of O4 (not apparent also in the NMR spectrum of γ-$ZrW_2{}^{17}O_8$ [48]) may be an indication that this terminal oxygen only reappears in the structure after the complete recrystallization.

In brief, within limits imposed by the experimental signal-to-noise ratio, no evidence of terminal oxygens was found in the analysis of the NMR data for samples of amorphous zirconium tungstate previously heated up to the threshold of recrystallization. This observation, which holds up no matter the details of postprocessing of NMR data, suggests that the irreversible structural relaxation of a-$ZrW_2{}^{17}O_8$ results from local atomic rearrangements, without breaking of the new W-O bonds formed on amorphization.

C. Vibrational spectroscopy

Figures 3 and 4 show the room-temperature Raman and far-infrared spectra of a-$ZrW_2{}^{17}O_8$, as produced and after annealing at increasingly higher temperatures, as well as after recrystallization into α-ZrW_2O_8.

Curiously, the Raman spectrum of a-ZrW_2O_8 exhibits two distinct peaks at 56 and 67 cm^{-1}. Vibrational modes of α-ZrW_2O_8 in this frequency range involve the concerted motion of first-coordination polyhedra, with large-amplitude translational/librational motion of the terminal oxygens [20]. In a-ZrW_2O_8, despite the absence of terminal oxygens, these well-defined Raman peaks suggest that there are still enough degrees of freedom in the local amorphous structure as to allow low-energy vibrational modes, in which first-coordination polyhedra behave as relatively rigid units. The peaks at 56 and 67 cm^{-1} seem to merge upon increasing annealing temperature while, concomitantly, a low-energy Raman peak at 40 cm^{-1} becomes apparent in the room-temperature Raman spectrum of the sample previously annealed at 620 °C.

In the Raman and far-infrared spectra of α-ZrW_2O_8 it is possible to observe a very distinct Raman peak/infrared band at 40 cm^{-1}, which has been previously assigned to a low-energy vibrational mode made possible by the presence

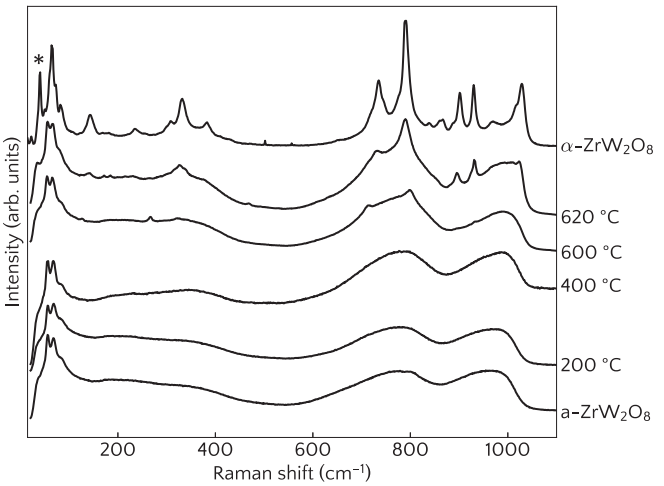

FIG. 3. Room-temperature, Raman spectra of α-ZrW_2O_8 (top) and of amorphous $ZrW_2{}^{17}O_8$, as amorphized and after thermal treatments at increasingly higher temperatures. The asterisk marks the Raman peak at 40 cm^{-1} assigned to a vibrational mode with large-amplitude motion of terminal oxygens [20].

of terminal oxygen atoms [20]. In fact, it has been shown that this band at 40 cm^{-1} can be assigned to a vibrational mode characterized by a significant translational motion of the WO_4 polyhedron and, therefore, is rather sensitive to the presence of terminal oxygens. In a-ZrW_2O_8, which has no terminal oxygen atoms, there is no hint of the presence of this band in either Raman or infrared spectra, even for samples previously heated up to 600 °C. The band at 40 cm^{-1} becomes apparent in the far-infrared spectrum of the sample previously heated up to 680 °C. Likewise, the corresponding peak can be seen in the Raman spectrum of the sample after annealing at 620 °C. In either Raman or far-infrared spectroscopy, evidence of terminal oxygens only becomes apparent when the sample was previously heated at temperatures above the recrystallization threshold of about 600 °C. Accordingly, results from vibrational spectroscopy analysis of a-ZrW_2O_8 suggest that the irreversible nature of the structural relaxation of amorphous zirconium tungstate is not a result of W-O bond breaking, thus

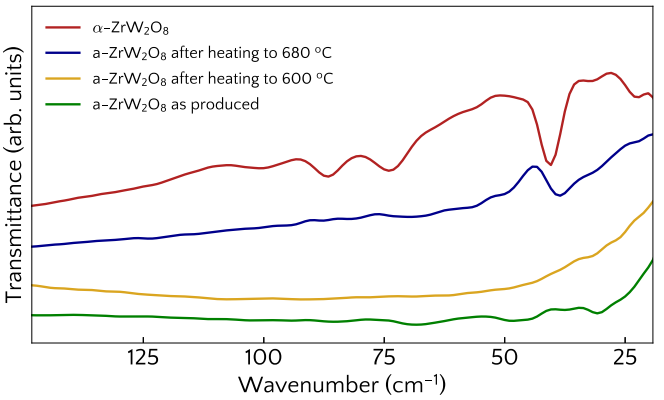

FIG. 4. Room-temperature, Fourier-transform far-infrared spectra of α-ZrW_2O_8 and a-$ZrW_2{}^{17}O_8$ as produced and after heating to 600 °C and 680 °C.

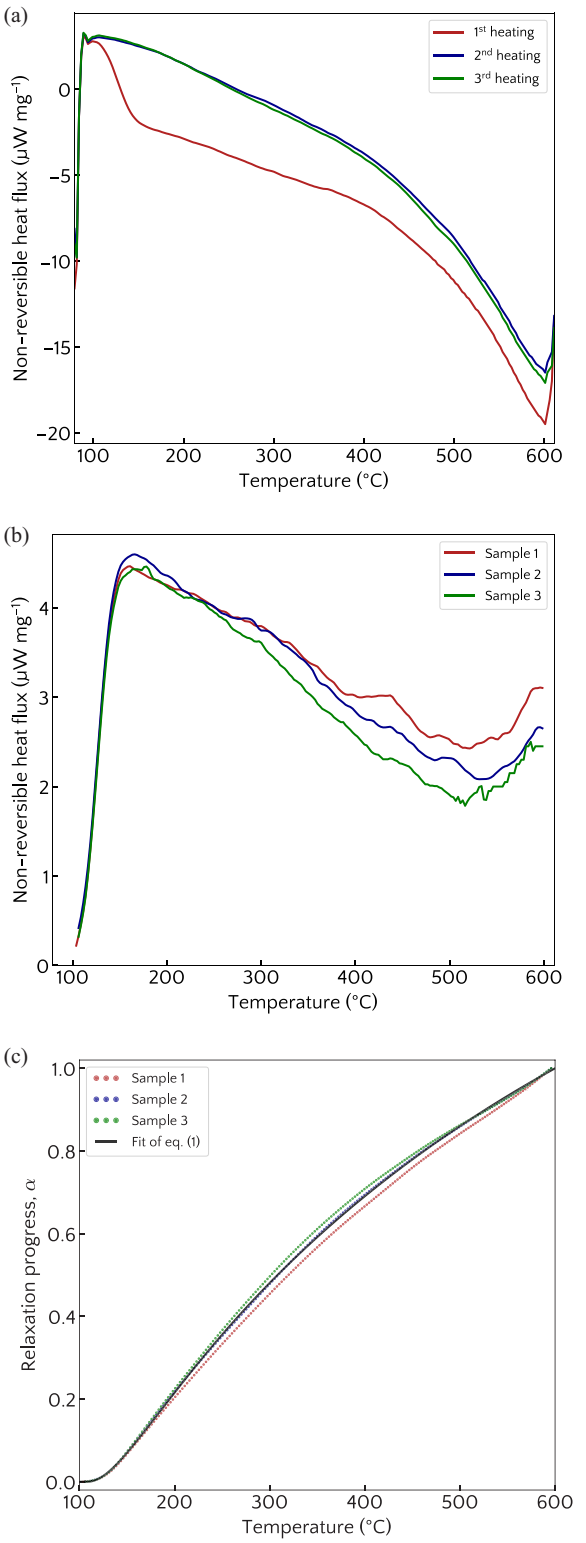

FIG. 5. (a) Nonreversible heat flux (exo down) from three consecutive TMDSC runs with the same sample of amorphous zirconium tungstate, (b) nonreversible heat flux (exo up) obtained after subtracting from nonreversible signal measured at the first TMDSC run the average nonreversible signal from the second and third runs, for each of the three samples of amorphous zirconium tungstate used in this work, and (c) progress of the structural relaxation of a-ZrW_2O_8 as a function of temperature for the three samples studied in this work, along with the fitting of Eq. (1).

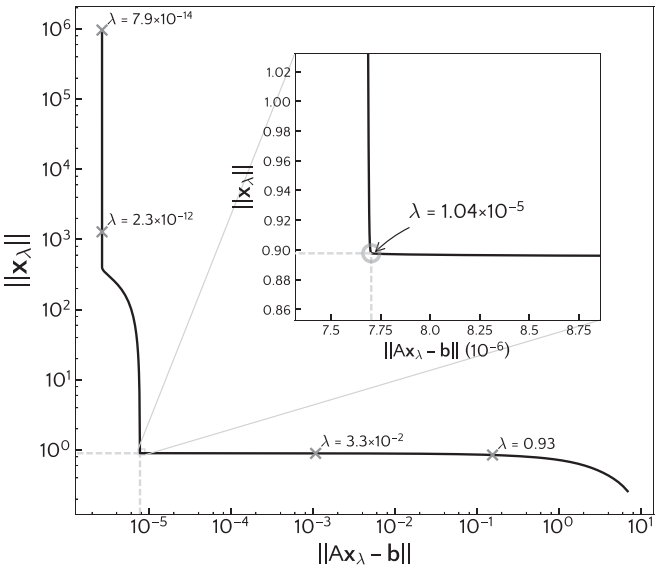

FIG. 6. *L*-curve plot for the determination of the regularization parameter λ.

corroborating the conclusion based on the analysis of ^{17}O MAS NMR data.

D. Spectrum of energy-distributed processes

Panel (a) of Figure 5 illustrates the nonreversible heat-flux signal from three consecutive runs with the same sample of amorphous zirconium tungstate. The nonreversible signals in the second and third scans were almost indistinguishable for all samples studied in this work, thus indicating that relaxation was essentially completed after the first heating run. Plotted in panel (b) is the nonreversible heat flux obtained after subtracting from the first MDSC run the average nonreversible signal from the second and third runs, for each of three different samples of amorphous zirconium tungstate. Finally, on the bottom panel of Fig. 5, the relaxation progress, α, is plotted as a function of temperature.

The *L*-curve plot, shown in Fig. 6, yields a regularization parameter $\lambda = 1.04 \times 10^{-5}$. The spectrum of activation energy for the irreversible structural relaxation of amorphous zirconium tungstate, as obtained by solving the inverse problem of Eq. (6) using Tikhonov's regularization, is shown in Fig. 7.

Also shown in Fig. 7 is the effect of the regularization parameter λ on the solution. A λ lower than optimum will give less weight to the norm of the solution vector, leading to a noisier solution. On the other hand, a λ higher than optimum yields a smoother solution, at the expenses of a larger residue. It is worth noting that the main features of the spectrum of activation energy for the structural relaxation of amorphous zirconium tungstate are rather insensitive on the choice of the regularization parameter, as shown in Fig. 7, where λ is changed over four orders of magnitude. In fact, in all the spectra depicted in Fig. 7, the number density of available processes is nearly uniformly distributed over the energy interval from 1 to 2.5 eV, slightly decreasing from a first maximum near 1.7 eV, and with a second maximum arising near the high-energy end of the activation energy spectrum. It is also worth noting that the nearly rectangular-shaped distribution of available processes

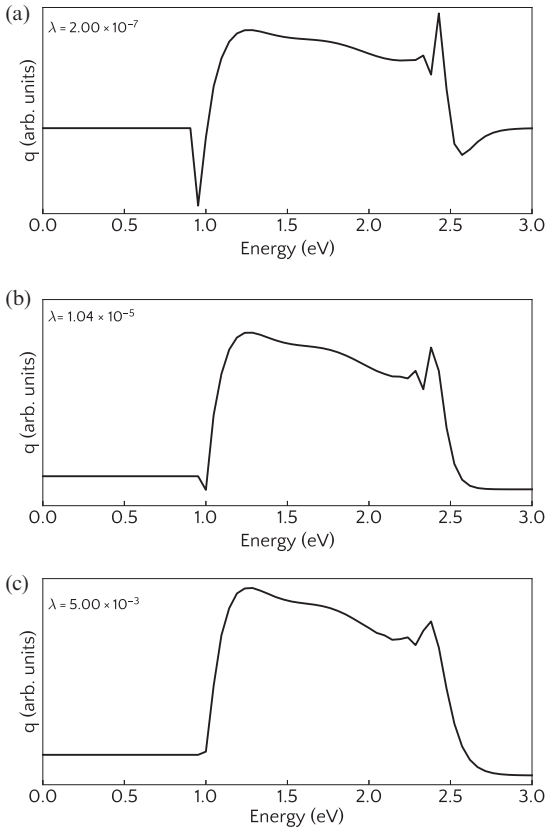

FIG. 7. Spectrum of activation energy for the irreversible structural relaxation of amorphous zirconium tungstate obtained as (a) a sub-regularized solution, (b) the optimum solution with λ chosen from the *L* curve, and (c) an over-regularized solution. In these panels, *q* represents the number density of available processes for structural relaxation.

over a relatively large energy interval resembles very much the almost uniform distribution of energy barriers between neighboring minima in the energy landscape of amorphous materials, as advanced by Anderson in the context of the two-level system model [49]. Indeed, elements of the two-level system model have been previously used in explaining several observations regarding relaxation phenomena in amorphous materials [50–54]. In the present case, the broad activation energy spectrum can be seen as a one-dimensional mapping of the complex energy configurational landscape of the ZrW_2O_8 amorphous phase, with its many thermally activated and mostly irreversible crossings between different, metastable, local atomic arrangements.

Once the activation energy spectrum is known, one can simulate the progress of the isothermal relaxation progress for an arbitrary temperature. Figure 8 shows the progress of the amorphous zirconium tungstate structural relaxation at increasingly higher temperatures up to the threshold of the recrystallization.

The structural relaxation of amorphous zirconium tungstate, as shown in Fig. 8, takes place up to a certain point even at relatively low temperatures, though with a very slow rate. At higher temperatures, the increased likelihood of the different local structural rearrangements accelerates the relaxation

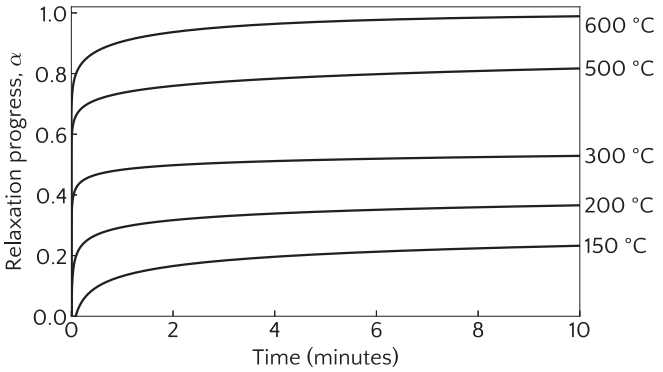

FIG. 8. Progress of the isothermal structural relaxation of amorphous zirconium tungstate simulated for different annealing temperatures.

process to the point that it is detectable in the time span of typical experiments. The local structure rearrangements are mostly irreversible and, therefore, as the temperature increases irreversible changes can be noted in several physical properties of amorphous zirconium tungstate [12,13,55]. It is worth mentioning that the progress of the structural relaxation at constant temperature shows a logarithmic dependence on time [30].

Finally, when the crystallization temperature is reached (i.e., above about 600 °C), enough thermal energy is available to break the new W-O bonds created during pressure-induced amorphization. This observation is supported by Raman and far-infrared spectroscopy results, as well as ^{17}O nuclear magnetic resonance, where conclusive evidence of terminal oxygen atoms is apparent only after the amorphous phase has been heated above the recrystallization temperature.

IV. CONCLUSIONS

MAS NMR ^{17}O analysis revealed no evidence of terminal oxygens in a-ZrW_2O_8 samples previously annealed up to 615 °C. The absence of terminal oxygen atoms in samples of amorphous zirconium tungstate, even after heating just below the recrystallization threshold, was corroborated by the lack of any evidence of the 40 cm^{-1} vibrational mode in both Raman and far-infrared spectra. The kinetics of the exothermic structural relaxation of amorphous zirconium tungstate could be well described by a continuous spectrum of activation energy, with thermally activated processes spanning all the interval from 1 to 2.5 eV. All these observations are consistent with a relaxation mechanism in which a-ZrW_2O_8 undergoes a series of mostly irreversible local atomic rearrangements, without bond breaking, with small clusters of atoms crossing from one local minimum energy configuration to another, in a possibly very complex energy landscape. The simulated progress of the isothermal structural relaxation of amorphous zirconium tungstate exhibits a logarithmic dependence on time, consistent with previous observations on the relaxation of other amorphous materials [30].

ACKNOWLEDGMENTS

Support from the Brazilian agencies Conselho Nacional de Desenvolvimento Científico e Tecnológico (CNPq) [Grants No. 472447/2011-4, No. 302928/2011-1 (C.A.P.), No. 304831/2014-0 (C.A.P.), No. 302289/2012-7 (J.E.Z.), and No. 304675/2015-6 (J.E.Z.)], Coordenação de Aperfeiçoamento de Pessoal de Nível Superior (CAPES), Secretaria de Desenvolvimento Econômico, Ciência, e Tecnologia do Estado do Rio Grande do Sul (SDECT/RS), Programa de Apoio a Núcleos de Excelência (PRONEX), and Fundação de Amparo à Pesquisa do Estado do Rio Grande do Sul (FAPERGS) is gratefully acknowledged. Thanks are also due to Netzsch Gerätebau GmbH (Germany), Jim Walker (Wah Chang Co., Albany, OR), for the sample of zirconium tungstate used in this work, Aline Lima de Oliveira (Universidade de Brasília, Brazil), who carried out the NMR measurements reported in this work, and the staff of the Instituto de Materiais Cerâmicos at the Universidade de Caxias do Sul, mainly Robinson C. D. Cruz and Daniel Golle.

[1] C. Martinek and F. A. Hummel, J. Am. Ceram. Soc. **51**, 227 (1968).
[2] T. A. Mary, J. S. O. Evans, T. Vogt, and A. W. Sleight, Science **272**, 90 (1996).
[3] A. P. Ramirez and G. R. Kowach, Phys. Rev. Lett. **80**, 4903 (1998).
[4] C. A. Kennedy and M. A. White, Solid State Commun. **134**, 271 (2005).
[5] F. R. Drymiotis, H. Ledbetter, J. B. Betts, T. Kimura, J. C. Lashley, A. Migliori, A. P. Ramirez, G. R. Kowach, and J. Van Duijn, Phys. Rev. Lett. **93**, 025502 (2004).
[6] C. A. Figueirêdo and C. A. Perottoni, Phys. Rev. B **75**, 184110 (2007).
[7] J. S. O. Evans, Z. Hu, J. D. Jorgensen, D. N. Argyriou, S. Short, and A. W. Sleight, Science **275**, 61 (1997).
[8] J. D. Jorgensen, Z. Hu, S. Teslic, D. N. Argyriou, S. Short, J. S. O. Evans, and A. W. Sleight, Phys. Rev. B **59**, 215 (1999).
[9] J. S. O. Evans, J. D. Jorgensen, S. Short, W. I. F. David, R. M. Ibberson, and A. W. Sleight, Phys. Rev. B **60**, 14643 (1999).
[10] C. A. Perottoni and J. A. H. da Jornada, Science **280**, 886 (1998).
[11] C. A. Perottoni, J. E. Zorzi, and J. A. H. da Jornada, Solid State Commun. **134**, 319 (2005).
[12] J. Catafesta, J. E. Zorzi, C. A. Perottoni, M. R. Gallas, and J. A. H. da Jornada, J. Am. Ceram. Soc. **89**, 2341 (2006).
[13] G. R. Ramos, J. Catafesta, J. E. Zorzi, J. A. H. da Jornada, and C. A. Perottoni, Phys. Rev. B **84**, 094121 (2011).
[14] A. W. Sleight, Annu. Rev. Mater. Sci. **28**, 29 (1998).
[15] A. K. A. Pryde, K. D. Hammonds, M. T. Dove, V. Heine, J. D. Gale, and M. C. Warren, J. Phys.: Condens. Matter **8**, 10973 (1996).
[16] M. T. Dove and H. Fang, Rep. Prog. Phys. **79**, 066503 (2016).
[17] M. G. Tucker, A. L. Goodwin, M. T. Dove, D. A. Keen, S. A. Wells, and J. S. O. Evans, Phys. Rev. Lett. **95**, 255501 (2005).
[18] D. Cao, F. Bridges, G. R. Kowach, and A. P. Ramirez, Phys. Rev. Lett. **89**, 215902 (2002).

[19] D. Cao, F. Bridges, G. R. Kowach, and A. P. Ramirez, Phys. Rev. B **68**, 014303 (2003).

[20] V. Gava, A. L. Martinotto, and C. A. Perottoni, Phys. Rev. Lett. **109**, 195503 (2012).

[21] M. K. Gupta, R. Mittal, and S. L. Chaplot, Phys. Rev. B **88**, 014303 (2013).

[22] A. Sanson, Chem. Mater. **26**, 3716 (2014).

[23] A. S. Pereira, C. A. Perottoni, and J. A. H. da Jornada, J. Raman Spectrosc. **34**, 578 (2003).

[24] S. M. Sharma and S. Sikka, Prog. Mater. Sci. **40**, 1 (1996).

[25] A. K. Arora, V. S. Sastry, P. C. Sahu, and T. A. Mary, J. Phys.: Condens. Matter **16**, 1025 (2004).

[26] A. Grzechnik, W. A. Crichton, K. Syassen, P. Adler, and M. Mezouar, Chem. Mater. **13**, 4255 (2001).

[27] K. Umemoto, R. M. Wentzcovitch, S. Baroni, and S. de Gironcoli, Phys. Rev. Lett. **92**, 105502 (2004).

[28] C. A. Figueiredo, J. Catafesta, J. E. Zorzi, L. Salvador, I. J. R. Baumvol, M. R. Gallas, J. A. H. da Jornada, and C. A. Perottoni, Phys. Rev. B **76**, 184201 (2007).

[29] J. H. Shin and H. A. Atwater, Phys. Rev. B **48**, 5964 (1993).

[30] M. Gibbs, J. Evetts, and J. Leake, J. Mater. Sci. **18**, 278 (1983).

[31] J. M. Gallardo-Amores, U. Amador, E. Moran, and M. A. Alario-Franco, Int. J. Inorg. Mater. **2**, 123 (2000).

[32] T. R. Ravindran, A. K. Arora, V. S. Sastry, and P. C. Sahu, J. Non-Cryst. Solids **355**, 2289 (2009).

[33] T. Varga, C. Lind, A. P. Wilkinson, H. Xu, C. E. Lesher, and A. Navrotsky, Chem. Mater. **19**, 468 (2007).

[34] W. Primak, Phys. Rev. **100**, 1677 (1955).

[35] M. E. Hochstenbach and L. Reichel, J. Integral Equ. Appl. **22**, 465 (2010).

[36] R. C. Aster, B. Borchers, and C. H. Thurber, *Parameter Estimation and Inverse Problems*, 2nd ed. (Elsevier/Academic Press, Amsterdam, 2013).

[37] C. Figueirêdo, M. Gallas, J. Zorzi, and C. Perottoni, J. Alloys Compd. **598**, 266 (2014).

[38] W. Sherman and A. Stadtmuller, *Experimental Techniques in High-Pressure Research* (John Wiley & Sons Incorporated, Chichester, 1987).

[39] M. Eremets, *High Pressure Experimental Methods*, Oxford Science Publications (Oxford University Press, Oxford, 1996).

[40] J. Rodriguez-Carvajal, in Abstracts of the Satellite Meeting on Powder Diffraction of the XV Congress of the IUCr, Toulouse, France, 1990, p. 127.

[41] M. R. Hampson, S. Allen, I. J. King, C. J. Crossland, P. Hodgkinson, R. K. Harris, F. Fayon, and J. S. O. Evans, Solid State Sci. **7**, 819 (2005).

[42] R. Storn and K. Price, J. Global Optim. **11**, 341 (1997).

[43] C. Baker, Expansion methods, in *Numerical Solution of Integral Equations* (Clarendon Press, London, 1974), Chap. 7, pp. 80–96.

[44] G. H. Golub, P. C. Hansen, and D. P. O'Leary, SIAM J. Matrix Anal. A **21**, 185 (1999).

[45] P. C. Hansen and D. P. O'Leary, SIAM J. Sci. Comput. **14**, 1487 (1993).

[46] P. C. Hansen, *The L-Curve and Its Use in the Numerical Treatment of Inverse Problems* (IMM, Department of Mathematical Modeling, Technical University of Denmark, Lyngby, 1999).

[47] P. C. Hansen, Numer. Algorithms **46**, 189 (2007).

[48] A. Soleilhavoup, M. R. Hampson, S. J. Clark, J. S. O. Evans, and P. Hodgkinson, Magn. Reson. Chem. **45**, S144 (2007).

[49] P. W. Anderson, B. I. Halperin, and C. M. Varma, Philos. Mag. **25**, 1 (1972).

[50] H. Kronmüller, Phys. Status Solidi B **118**, 661 (1983).

[51] A. P. Paz, I. V. Lebedeva, I. V. Tokatly, and A. Rubio, Phys. Rev. B **90**, 224202 (2014).

[52] G. Hygate and M. R. J. Gibbs, J. Phys.: Condens. Matter **2**, 1425 (1990).

[53] P. Fantini, M. Ferro, and A. Calderoni, Appl. Phys. Lett. **102**, 253505 (2013).

[54] W. A. Phillips, Rep. Prog. Phys. **50**, 1657 (1987).

[55] R. F. L. Lorenzi, J. E. Zorzi, and C. A. Perottoni, J. Non-Cryst. Solids **403**, 102 (2014).